Dynamic Fluid Surface Reconstruction Using Deep Neural Network Supplementary Material

Simron Thapa Nianyi Li Jinwei Ye
Louisiana State University, Baton Rouge, LA 70803, USA
{sthapa5, nli5, jinweiye}@lsu.edu

In this supplementary material, we provide more details on our network structures and the wave equations for fluid surface modeling. We also include additional experimental results.

1. Detailed Network Architecture

Our *fluid surface reconstruction network (FSRN)* consists of two sub-nets: 1) an encoder-decoder based convolutional neural network (FSRN-CNN) for per-frame depth and normal estimation and 2) a recurrent neural network for enforcing the temporal consistency across multiple frames (FSRN-RNN). Table 1 and Table 2 provide detailed network architecture of the two subnets.

Input	Filters	Output size
Input		$128 \times 128 \times 6$
Conv+Conv	$18@2 \times 2 \times 6$	$128 \times 128 \times 18$
Maxpool	Stride = 2	$64 \times 64 \times 18$
Conv+Conv	$36@2 \times 2 \times 18$	$64 \times 64 \times 36$
Maxpool	Stride = 2	$32 \times 32 \times 36$
Conv+Conv+Conv	$72@2 \times 2 \times 36$	$32 \times 32 \times 72$
Maxpool	Stride = 2	$16 \times 16 \times 72$
Conv+Conv+Conv	$144@2 \times 2 \times 72$	$16 \times 16 \times 144$
Maxpool	Stride = 2	$8 \times 8 \times 144$
Conv+Conv+Conv	$144@2 \times 2 \times 144$	$8 \times 8 \times 144$
Maxpool	Stride = 2	$4 \times 4 \times 144$
Deconv	$72@4 \times 4 \times 144$	$8 \times 8 \times 72$
Concat+Deconv	$36@6 \times 6 \times 72$	$16 \times 16 \times 36$
Concat+Deconv	$18@4 \times 4 \times 36$	$32 \times 32 \times 18$
Concat+Deconv	$9@4 \times 4 \times 18$	$64 \times 64 \times 9$
Concat+Deconv	$4@3 \times 3 \times 9$	$128 \times 128 \times 4$
Output_1		$128 \times 128 \times 4$
Deconv	$72@4 \times 4 \times 144$	$8 \times 8 \times 72$
Concat+Deconv	$36@6 \times 6 \times 72$	$16 \times 16 \times 36$
Concat+Deconv	$18@4 \times 4 \times 36$	$32 \times 32 \times 18$
Concat+Deconv	$9@4 \times 4 \times 18$	$64 \times 64 \times 9$
Concat+Deconv	$1@3 \times 3 \times 9$	$128 \times 128 \times 1$
Output_2		$128 \times 128 \times 1$

Table 1. Detailed network architecture of FSRN-CNN.

Input	Filters	Output size
Input		$3 \times 128 \times 128 \times 4$
convLSTM	$4@2 \times 2 \times 4$	$3 \times 128 \times 128 \times 4$
convLSTM	$4@2 \times 2 \times 4$	$3 \times 128 \times 128 \times 4$
convLSTM	$4@2 \times 2 \times 4$	$128 \times 128 \times 4$
Conv	$4@2 \times 2 \times 4$	$128 \times 128 \times 4$
Output		$128 \times 128 \times 4$

Table 2. Detailed network architecture of FSRN-RNN.

2. Wave Equations for Fluid Modeling

In this section, we provide details of the wave equations that we use for fluid modeling when creating the physics-based fluid dataset. We incorporate four types of wave equations: the shallow water wave equations, Grestner's wave equations, Gaussian equations, and sinusoidal equations.

The shallow water wave equations are a set of partial differential equations derived from the Navier-Stokes [1]. They describe in-compressible property of fluid where the mass and linear momentum is conserved. Let z_{sh} be the fluid surface height, (x, y) be the Eularian mesh grid and t be the time instant, the differential equations can be written as

$$\begin{cases} \frac{\partial(\rho z_{sh})}{\partial t} + \frac{\partial(\rho z_{sh} u)}{\partial x} + \frac{\partial(\rho z_{sh} u)}{\partial y} = 0 \\ \frac{\partial(\rho z_{sh} u)}{\partial t} + \frac{\partial}{\partial x}(\rho z_{sh} u^2 \frac{1}{2} \rho g z_{sh}^2) + \frac{\partial(\rho z_{sh} uv)}{\partial y} = 0 \\ \frac{\partial(\rho z_{sh} v)}{\partial t} + \frac{\partial(\rho z_{sh} uv)}{\partial x} + \frac{\partial}{\partial y}(\rho z_{sh} v^2 \frac{1}{2} \rho g z_{sh}^2) = 0 \end{cases} \tag{1}$$

where (u, v) is the 2D velocity, ρ is the fluid density and g is the gravity acceleration constant.

The Grestner's wave equations are are widely used in computer graphics to simulate ocean waves [2]. We use them to model fluid with relatively large volumes. In our implementation, we compute the Grestner's equation with its Fast Fourier Transform (FFT) form. The FFT-based representation of the equation can be written as

$$z_{gr} = \sum_m \sum_n \tilde{z}_{gr} \exp(j 2\pi (mx + ny)) \tag{2}$$

where $\tilde{z}_{gr}$ is the Fourier amplitude, j is the imaginary unit, m and n are integers bounded by $[-M/2, M/2]$ and $[-N/2, N/2]$ (M and N are the dimensions of the mesh grid). We use the Phillips spectrum [2] as our height amplitude Fourier component ($\tilde{z}_{gr}$) that determines the structure of the fluid surface.

Gaussian equations are used for creating water ripples with damping effects. Let z_{ga} be the fluid surface height, the equation can be written as

$$z_{ga} = A \exp(-\frac{x^2 + y^2}{2\sigma^2}) \sin(\omega t) \tag{3}$$

where A is the wave amplitude, σ is the damping factor, and ω is the phase factor.

Sinusoidal wave equations provide good approximation for the fluid dynamics. We use them to model linearly propagating waves. Let z_{si} be the fluid surface height, the equation can be written as

$$z_{si} = \sum_i A_i \sin \frac{2\pi}{\lambda_i}(x + c_i t) \tag{4}$$

where A_i is the wave amplitude, λ_i is the wavelength, and c_i is the phase constant with respect to time.

The overall wave equation for modeling the fluid surface is a weighted linear combination of Equation 1 - Equation 4 and is written as

$$z = \zeta_1 z_{sh} + \zeta_2 z_{gr} + \zeta_3 z_{ga} + \zeta_4 z_{si} \tag{5}$$

where $\zeta_{1,\ldots,4}$ are weight coefficients. We are able to create various types wave that are physically realistic with Equation 5.

3. Additional Results

In this section, we show additional experimental results. Fig. 1 shows the visual comparisons of recovered depth and normal maps for the ablation study. Fig. 2 shows additional synthetic results. Fig. 3 shows additional real results. Please see the supplementary video for complete result sequences.

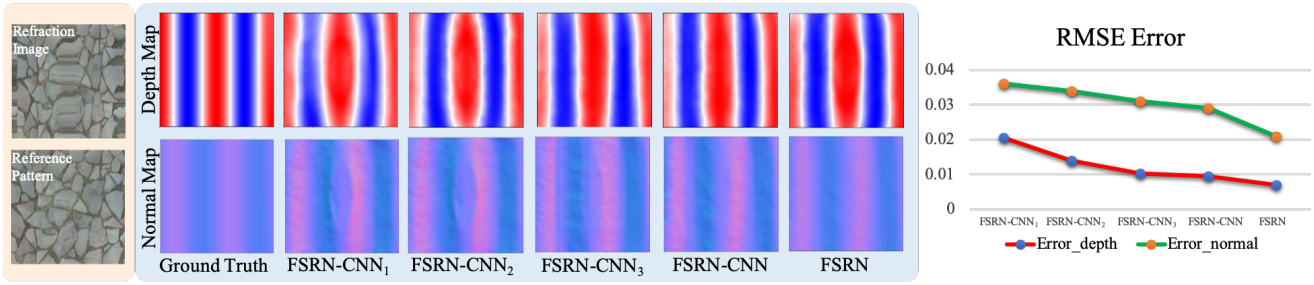

Figure 1. Visual comparisons for the ablation study. Left: we show the input refraction image and the original reference pattern. Middle: the recovered depth and normal maps of our network variants in comparison with the ground truth ones. Right: RMSE error plot for the network variants. We can see that the errors (for both depth and normal) decrease, as we incorporate more components in the loss function as well as using the RNN subnet.

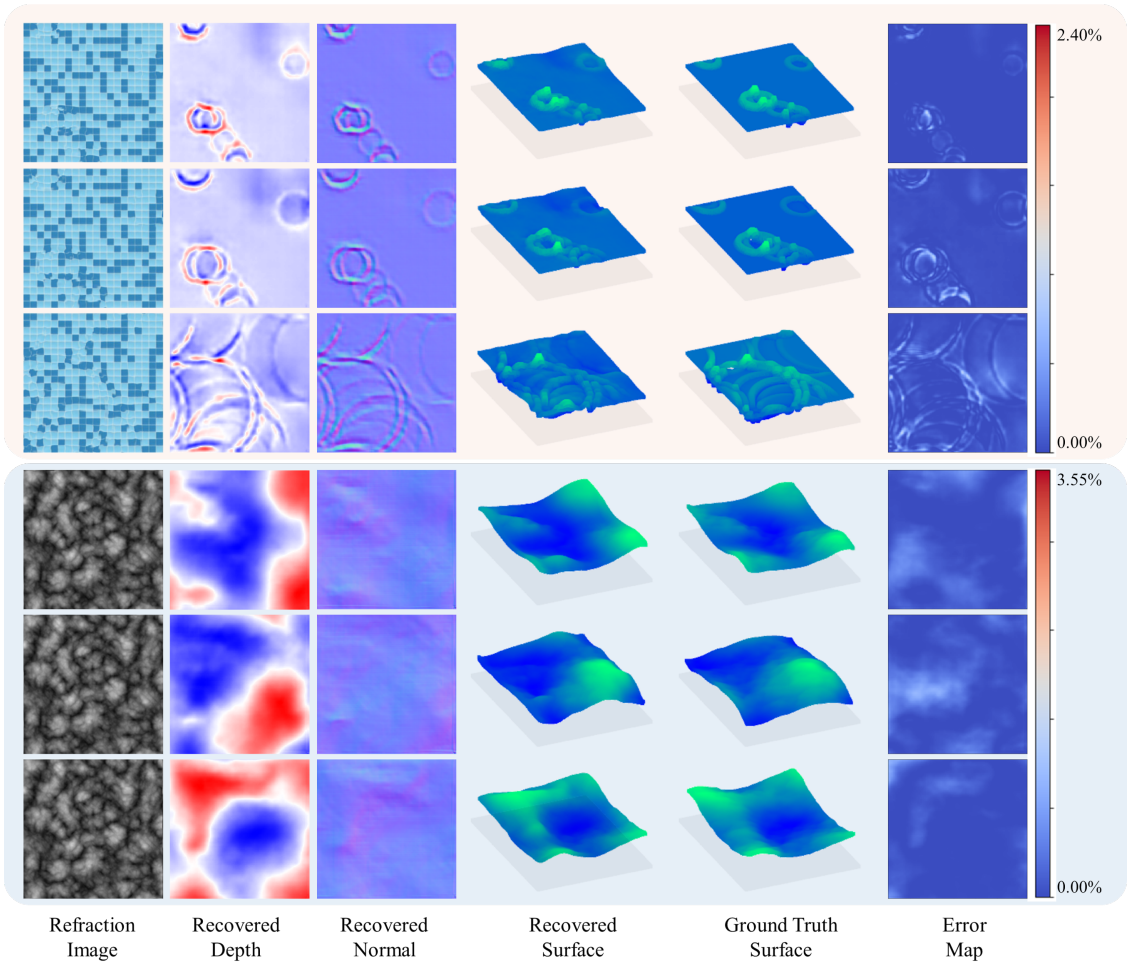

Figure 2. Additional results on synthetic data.

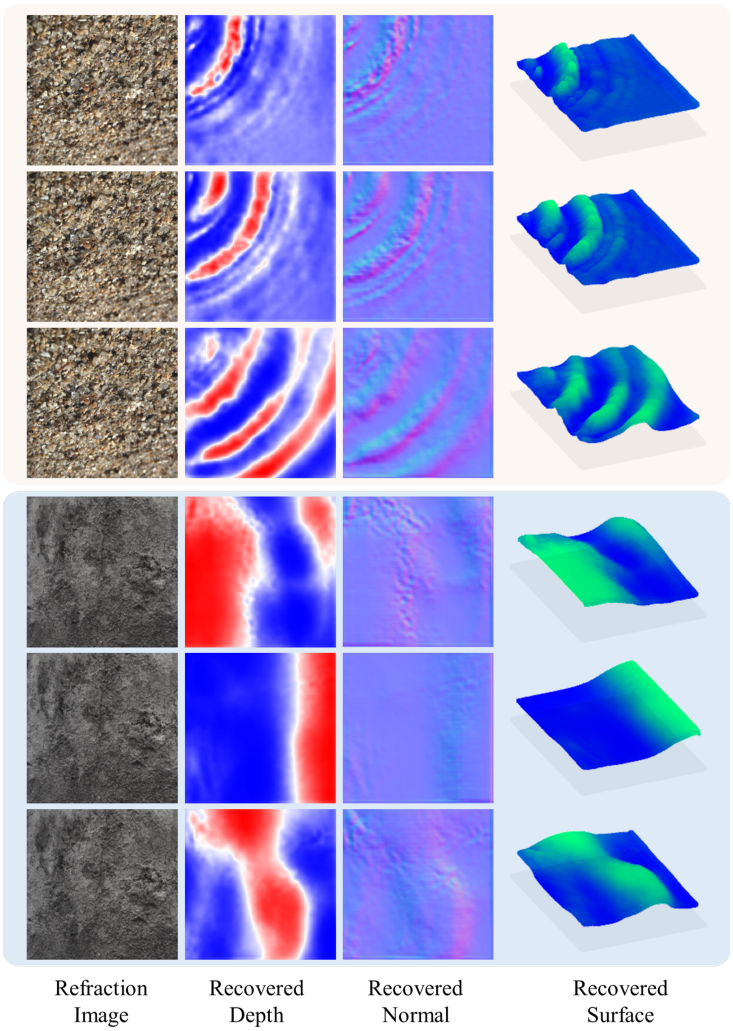

Figure 3. Additional results on real data.

References

[1] Adrian Constantin and Joachim Escher. Wave breaking for nonlinear nonlocal shallow water equations. *Acta Mathematica*, 181(2):229–243, 1998. 2

[2] Jerry Tessendorf. Simulating ocean water. *Simulating Nature: Realistic and Interactive Techniques. SIGGRAPH*, 1(2):5, 2001. 2